

# Gas flow and related beam losses in the ITER neutral beam injector

A. Krylov<sup>1,\*</sup> & R.S. Hemsworth<sup>2</sup>

<sup>1</sup>*Kurchatov Institute, pl. Kurchatova,1, Moscow 123182, Russia,*

<sup>2</sup>*Association EUROATOM-CEA, CEA/DSM/DRFC, CEA-Cadarache13108 St Paul-lez-Durance, France*

---

\*Corresponding author. Tel.: +33-4-4225-4523; fax.: +33-4-4225-62-33  
E-mail address: krylov@fusion.ru (A. Krylov)

**This paper has been submitted for publication to Fusion Engineering and Design**

---

## Abstract

The gas flow in the ITER neutral beam injectors has been studied using a 3D Monte-Carlo code to define a number of key parameters affecting the design and operation of the injector. This paper presents the results of calculations of the gas density in the two accelerator concepts presently considered as options for the ITER injectors, and the resultant stripping losses of the negative ions during their acceleration to 1 MeV. The sensitivity of the model to various parameters has been studied, including the gas temperature in the ion source and the subsequent accommodation by collisions with the accelerator structure, and the degree of dissociation of the D<sub>2</sub> or H<sub>2</sub> in the ion source, and subsequent recombination during collisions with the accelerator structure. Additionally the sensitivity of the losses to details of the beam source design and operating parameters are examined for the both accelerator concepts. © 2005 Published by Elsevier Science B.V.

*Keywords:* ITER, Neutral beam, Gas flow, Injector

---

# 1 Introduction

The design of the Neutral Beam Injectors (NBI's) for the International Thermonuclear Experimental Reactor (ITER) was carried out between 1995 and 2001 by the combined efforts of the interested ITER Home Teams (Europe, Japan and Russia) and the ITER Joint Central Team. The injector is designed to provide  $\approx 17$  MW of power, in the form of 1 MeV deuterium atoms, to the tokamak plasma during 1000 s, or even longer pulses (up to 3600 s). The design at all stages was affected, to a large extent, by considerations related to the gas flows in the injector. Gas flow considerations have dominated the overall design of the injector because of the necessity to keep the injector compact, in particular to limit the length of the injector, hence that of the proposed gas neutraliser. The latter consideration has led to the subdivision of the gas neutraliser into 4 vertical channels, with consequent restrictions on the beam geometry and optics. However, the most significant "physics" consideration is the loss of negative ions during acceleration by stripping on the gas escaping from the ion source. This paper presents the results of detailed calculations using a specially adapted 3D Monte Carlo code which can take into account heating and/or dissociation of the gas in the ion source. A general description of the latest design of the ITER injectors can be found in [1,2,3,4].

A simplified schematic of the gas flow in the injector is shown in Fig.1. Gas ( $H_2$  or  $D_2$ ) is fed to the ion source for generation of the negative ions ( $D^-$  or  $H^-$ ) and to the neutraliser to provide the gas target needed to convert the accelerated negative ions to fast atoms. Gas other than that converted to beam particles is pumped by cryopumps lining the walls of the injector and only a small part of the total gas feed to the injector flows to the tokamak.

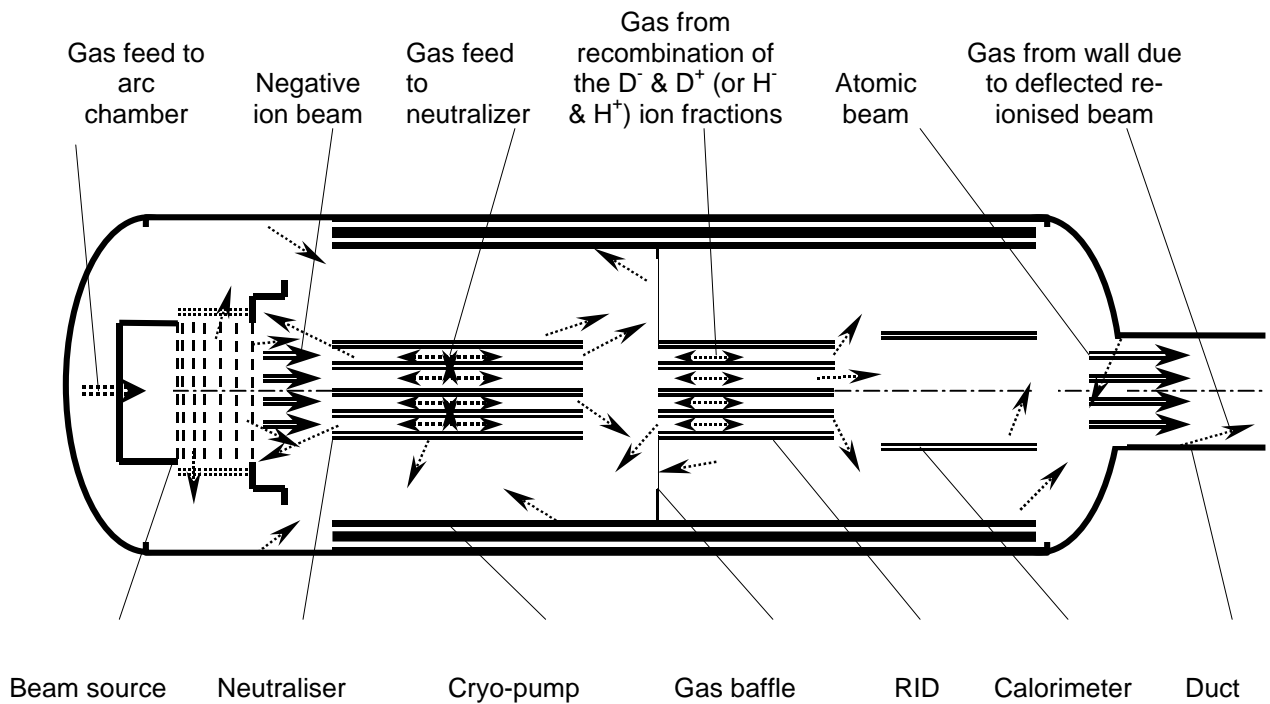


Fig.1. The gas flow in the ITER NBI (shown with the MAMuG accelerator). The gas flow created by direct beam interception is not indicated. The dashed narrows indicate the possible gas flow directions.

The gas feed to the neutraliser is defined by the geometry of the neutraliser and the target thickness required to obtain the optimum (i.e. maximum) neutralisation of the accelerated 1 MeV  $D^-$  ion beam, which is calculated (from cross section data) to be  $1.4 \times 10^{20} \text{ m}^{-2}$ . The maximum fraction of neutrals is  $\approx 60\%$ ; the rest consists of  $\approx 20\%$  negative and  $\approx 20\%$  positive ions. Ions leaving the neutraliser are deflected and then intercepted in the residual ion dump (RID) and recombine to produce a molecular gas flow inside the RID.

## 2 Beam source and calculation model

The beam source (BS) consists of the ion source (arc chamber and extractor), where negative ions are generated and extracted, and the accelerator, where the energy of the negative ions is increased to 1 MeV. The extraction and acceleration system has to form the beam in a way so as to provide the required beam emittance. There are two candidates for the accelerator: The MAMuG accelerator (the Multi Aperture Multi Grid accelerator) [5], which is being developing by JAERI, Japan, and the SINGAP accelerator (the SINGLE APerture or SINGLE GAP accelerator) [6], which is under development in the DRFC, CEA, France. Fig. 2 shows the reference (Kamaboko [7] type) negative ion source with both variants of the accelerator. The choice between the accelerator concepts has not yet been made and therefore the analysis presented below has been carried out for both options.

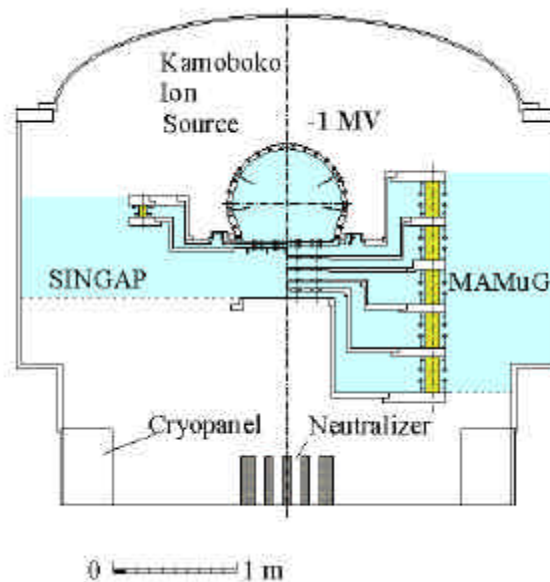


Fig.2. ITER beam source and part of the beamline. The left hand side corresponds to the BS with the SINGAP accelerator, the right hand side with the MAMuG accelerator. The shaded area is the region covered by the calculations reported in this paper. In both variants the accelerators are “vacuum” insulated, i.e. vacuum is

the insulating medium between the beam source structure and the ground potential vacuum chamber wall. This allows gas to flow laterally as well as axially (with the accelerated beam) out of the accelerator.

The 3D Monte Carlo code used for the calculations reported here is based on the code first developed for calculations of the gas density distribution in the ITER beam line. The code has been enhanced and used to obtain detailed results for both candidate accelerators for ITER. The BS geometry was taken from the ITER NBI final (2001) drawings, including the complicated shape of the apertures in the extractor(s). The dependence of the gas density and flow distributions were studied as a function of:

- the electrode and aperture geometry;
- the temperature of the gas in the arc chamber;
- the dissociation fraction in the arc chamber;
- the recombination coefficient of the atomic fraction on the electrodes and walls;
- the temperature(s) of the accelerator electrodes and the walls;
- the accommodation of molecular energy in collision with the electrodes and walls;
- the transparency of the electrode support structure for lateral gas flow;
- the isotope used ( $H_2$  or  $D_2$ ).

The code calculates the gas density resulting from the flow of slow D (or H) atoms and  $D_2$  (or  $H_2$ ) molecules out of the ion source. This gas density is used to calculate the stripping loss and the generation of secondary particles in the accelerator due to collisions of beam particles with the gas. The results were used to optimise the design and to compare the performance of the two accelerator concepts studied.

### 3 Calculation model

The space in the beam source available for gas flow was subdivided into a number of separate, simple, volumes of three types: a semi-cylindrical volume to represent the arc chamber, conical or cylindrical volumes to make up the apertures in the electrodes, and rectangular volumes to simulate the gaps between the electrodes and to simulate the electrode support structure. The large free space between the accelerator and the injector walls and the large main SINGAP gap were described as a number of adjacent volumes. The total model is constructed from these "elementary" volumes, each volume having the appropriate, specific, properties such as size and conditions at their boundaries (transparency, temperature, accommodation coefficient, etc.). Reflection from solid surfaces was always randomised in accordance with the cosine law. The typical pressures in the beam source lie between 0.03 and 0.3 Pa, so that the mean free path of the gas particles is between 4 and 40 cm. With the pressures and sizes in the system, "molecular" flow conditions can be assumed to apply everywhere downstream of the arc chamber. Therefore only collisions with solid walls are considered. This significantly simplified and shortened the calculation times.

In the calculation a probe molecule is generated at a random position in the arc chamber and tracked until it exited from the last electrode or crossed the lower boundary of the BS, the

dashed line in Fig. 2. Tracing the probe molecules until they are trapped on the cryo-pump is not necessary since previous calculations of the gas flow in the beam line have shown that the gas feed to the neutraliser is much higher than that to the BS (typically  $12 \div 14$  Pa.m<sup>3</sup>/s against  $1 \div 2$  Pa.m<sup>3</sup>/s), so it is mainly the flow from the neutraliser that defines the background pressure between the BS and the neutraliser,  $\approx 0.015$  Pa. This pressure was taken into account in the final pressure calculation (density distributions) by simply adding this pressure to the pressure throughout the BS.

Whilst the probe molecule is tracked inside of BS, the time spent in each volume traversed by the probe molecule was recorded in individual counters. These times were finally recalculated to statistically average the density in each of the individual volumes.

Due to the symmetry of the BS about both the vertical axis and its equatorial plane, only a quarter of the BS is described in the code, using mirror reflection at the point that a particle would pass through a symmetry plane. Fig. 2 is drawn approximately to scale and gives a general view of the model used. A molecule experiences typically 300 (SINGAP) to 500 (MAMuG) collisions before it leaves the BS. During this time the molecule returns back to the arc chamber 3 to 5 times. The typical number of probe molecules used was 32000, which provided the necessary statistical accuracy. Finally the calculated gas density distribution and gas flow rate from the BS have been normalised to have a source filling pressure of 0.3 Pa.

## 4 Results

Before using the model on the complex geometry of the BS, it was first validated by calculation of simple models that could be been verified by comparison with "classical" cases where the Knudsen formula of gas conductance can be applied. Agreement within 5% was demonstrated.

In actual operation of a BS, the gas flow rate,  $Q$ , into the ion source is adjusted (empirically) in such a way as to have the optimum performance of the ion source, which usually corresponds to the maximum accelerated negative ion beam current. The flow rate is fixed during BS operation. As the gas temperature and plasma flow inside the ion source during operation are not necessarily known, nor necessarily uniform, the concept of operating pressure cannot be easily defined. Hence it is usual to define the optimum conditions in terms of the "filling" pressure,  $P_f$ , i.e. the pressure in the ion source with no arc discharge and the ion source and accelerator at room temperature. It is presently assumed that for the ITER ion source this filling pressure will be 0.3 Pa; the gas density in the ion source is then  $7.4 \times 10^{19}$  m<sup>-3</sup>. The "filling" flow rate,  $Q_f$ , depends only on the geometry of the BS, and during these calculations this is adjusted each time the geometry of the BS has been varied to keep  $P_f$  at 0.3 Pa. Equation 1 relates the flow rate with a fixed geometry, the "filling" density,  $N_f$ , the arc chamber volume,  $V_{ch}$ , and the residence time of the molecules in the ion source,  $\hat{t}_f$ ,

$$Q_f = \frac{V_{ch} * N_f}{t_f} \quad (1)$$

When calculations were done for a gas temperature other than room temperature, the calculated density in the arc chamber was defined through the new calculated residence time,  $\hat{t}_f$ , by equation 2.

$$N = \frac{N_f * t}{t_f} \quad (2)$$

Then the densities in the downstream volumes were re-normalised by the ratio  $N/N_f$ .

The calculated gas density distributions in the MAMuG and SINGAP accelerators, obtained for the basic filling conditions, room temperature and  $P_f = 0.3$  Pa, are shown in Fig. 3.

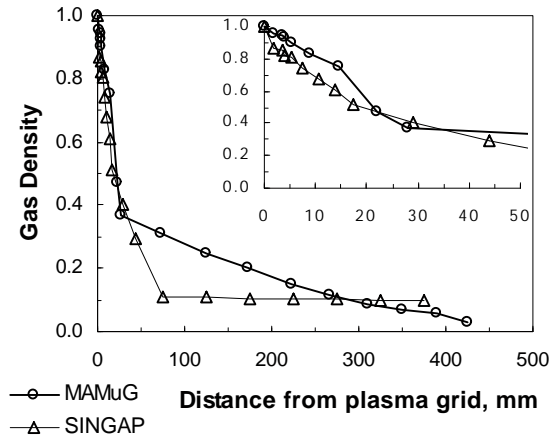


Fig. 3. Normalised gas density distributions in the MAMuG and SINGAP accelerators with all components at room temperature, 293 K. Here and in subsequent figures, each point on the curve corresponds to the result from a single “elementary” volume.

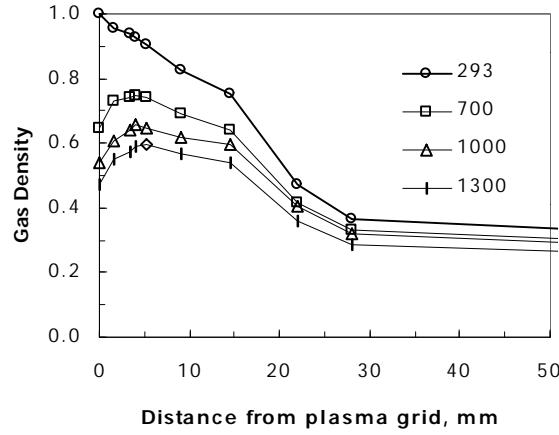
In both cases the density drops sharply in the extractor, i.e. the plasma grid and the extractor grid, and it is almost the same in both cases. This is because of the low conductance of the extractor, mainly that of the apertures in the electrodes, which are essentially the same in the two cases. (The gap between these electrodes is small and the grids are large, so the lateral conductance is negligible.)

#### 4.1 Sensitivity to the source gas temperature

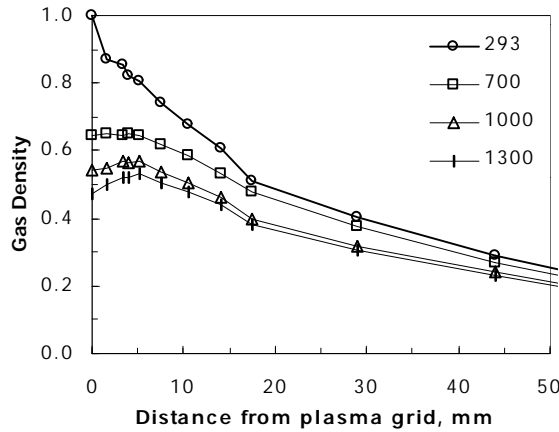
There is experimental evidence [8,9] that the gas in the ion source is heated significantly during source operation. Therefore gas density profiles have been calculated for gas temperatures above room temperature, in the range expected, i.e. up to 1300 K. Since the velocity of the molecules,  $V$ , increases as the gas temperature,  $T_{gas}$ , increases ( $V \propto T_{gas}^{1/2}$ ), with a fixed flow rate and molecular flow conditions (see above) the gas density in the ion source and the accelerator must decrease as the gas temperature increases, i.e. the conductance increases with temperature. If the temperature accommodation coefficient of the molecules impinging on the surfaces of the BS is greater than 0, the density profile can have a maximum downstream of the ion source due to gas cooling. Fig. 4 shows the initial part of density profiles for different temperatures of the gas leaving the ion source assuming a temperature accommodation coefficient,  $K_{ac}$ , of 0.2. Note that the pressure (not shown) decreases monotonically, like density in Fig. 3, but the density profiles are shown here as it is the density that influences directly the negative ion rate, not pressure.

It is foreseen to maintain the plasma grid of the ITER BS at  $\approx 300^\circ\text{C}$  as it has been found that this is needed to optimise the extracted negative ion current. For technical reasons the extraction and acceleration grids of the ITER BS will be cooled with water with a temperature close to  $100^\circ\text{C}$  [5]. Therefore in the calculations presented below the plasma grid temperature is set to  $300^\circ\text{C}$ , and all other grids and the grid support structure are set to  $100^\circ\text{C}$ .

One can see from the results shown in Fig. 4 that with the gas in the ion source at  $1000\text{ K}$ , the calculated density in the source is lower than “filling” one by  $0.55$ , which is, as expected, close to the square root of the ratio of the gas temperatures,  $(293/1000)^{1/2}$ .



a)



b)

Fig. 4. Normalised gas density distribution at different gas temperatures in the arc chamber. a) for the MAMuG accelerator, b) for the SINGAP accelerator.

Leaving aside any possible variation of the extracted negative ion current with the pressure (gas density) in the ion source, the minimum value of the stripping loss,  $L_s$ , serves as a figure of merit for the gas flow conditions in the BS. The stripping loss along the negative ion trajectory between the ion source plasma to the exit from the accelerator is given by:  $L_s = \int \bar{\sigma} N(x) \phi_{-10}[E(x)] dx$ . Note that both the gas density,  $N$ , and the energy of negative ions,  $E$ , depend on the distance from the ion source plasma,  $x$ , and that the stripping cross section,  $\phi_{-10}$ , varies with  $E$ . Strictly speaking  $L_s$  depends also on the distance of the ion from the beam axis as the gas density varies across the beam (see also Fig. 6 below).

The decrease of the  $D^-$  current due to stripping in the accelerator is shown in Fig. 5. The calculation of the stripping loss takes into account that the density between the surfaces of opposing grids does not vary significantly, whereas the energy of the ions increases almost linearly between the grids, and that the inverse occurs in a long aperture in thick grids. The density profiles shown in Fig. 5 are not smoothed, but shown as calculated. The energy profiles for the MAMuG and SINGAP geometries were taken from [10]. The cross sections used were calculated using the Chebyshev fitting coefficients taken from the Oak Ridge “Red Book” [11].

Fig. 5 shows that with the same conditions (source filling pressure and gas and electrode temperatures), the SINGAP option provides a better beam generation efficiency by  $\approx 15\%$ .

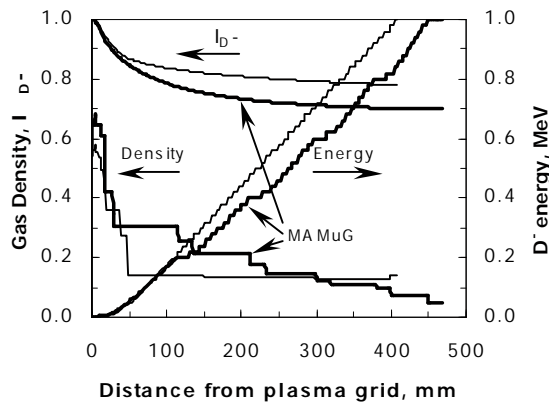


Fig. 5. Normalised gas density distribution,  $D^-$  energy and relative current in the MAMuG and SINGAP accelerators. The temperature of the gas in the ion source was taken as 1000 K.

The following sections examine the stripping loss as function of a number of parameters. Amongst them are: accommodation of molecule on surfaces, gas temperature in the ion source, the lateral conductance and the transparency of the support structure, and some additional subjects.

#### 4.2 Sensitivity to the temperature accommodation coefficient

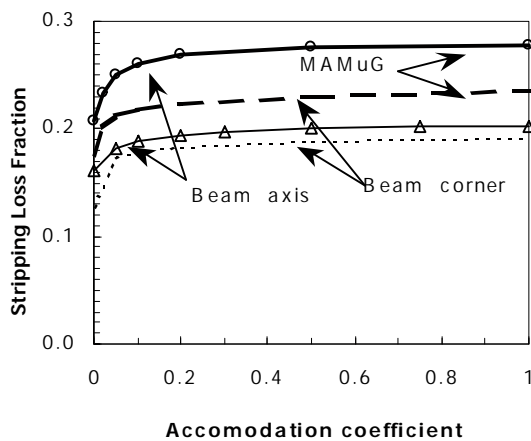


Fig. 6. Stripping loss as a function of the accommodation coefficient,  $K_{ac}$ , with  $T_{gas} = 1000$  K.

The accommodation coefficient of the molecules,  $K_{ac}$ , in collision with a surface, having a temperature  $T_w$  determines the “temperature” of the molecule after the collision:  $T_{m1} = T_w + (T_{m0} - T_w) * (1 - K_{ac})$ , where  $T_{m0}$  and  $T_{m1}$  are the “temperatures” of the molecule before and after the collision. The molecular velocities after collisions,  $V_{m1}$ , were calculated from the temperatures using:  $V_{m1} = (8kT_{m1}/\pi M)^{1/2}$ , where  $k$  is Boltzmann's constant and  $M$  is the mass of the molecule. The velocity direction was randomly chosen following the cosine distribution law.

The calculated stripping loss for various values of  $K_{ac}$  are shown in Fig. 6 at the beam axis and at the corner of the beam. The difference between these two locations arises because the pressure along the beam path is different at different transverse positions, see section 4.3 below.

For these calculations the following were assumed: plasma grid had temperature 573 K, the temperature of the acceleration grids and their support structure was 373 K. The walls of injector were assumed to be at 293 K.

It can be seen from Fig. 6 that the stripping loss is almost constant for  $K_{ac} \geq 0.2$ , which indicates that the molecules have, on average, 5 collisions with a grid or grid support before participating in the stripping process. Note that the total number of collisions experienced by an average molecule until exiting the BS is much greater: 350 to 400 with the SINGAP accelerator and 400 to 500 with the MAMuG accelerator. During its life in the BS the molecule exits and then returns back to the arc chamber several times,  $\sim 3$  times with the SINGAP accelerator and 4 to 5 times with the MAMuG accelerator. Many tens of collisions in the first extraction gap reliably cool the molecules down to the temperature of the grids. As a result the stripping decreases only slowly with increasing gas temperature in the arc chamber, see Fig. 7.

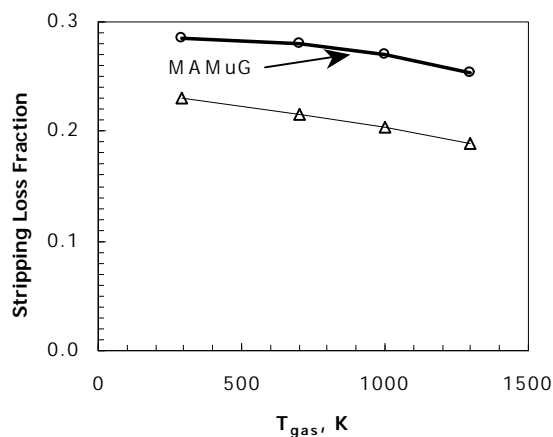
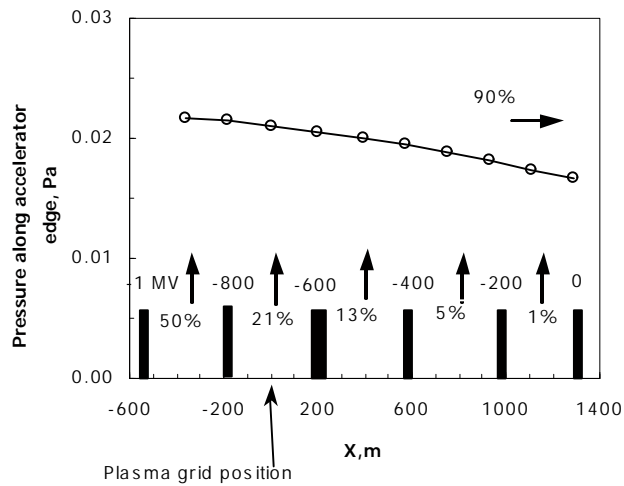
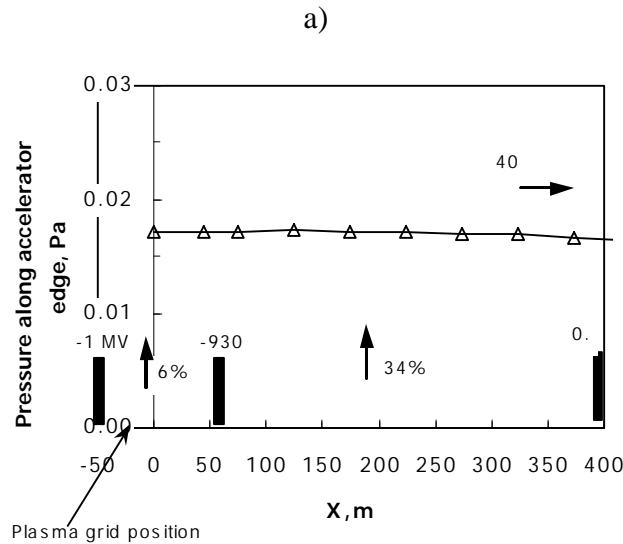


Fig. 7. Stripping loss as a function of the gas temperature in the arc chamber,  $T_{gas}$ , with  $K_{ac} = 0.2$ .

### 4.3 Gas flow, lateral pumping and stripping loss variation across the beam

Because part of the gas from the source leaves the beam path laterally, there is a density gradient from the centre to the edge of the accelerator. The density maximum within the beam path, hence the maximum stripping loss, occurs at the centre of the beam, and the density minimum within the beam path, hence the minimum loss, occurs at the corner of the beam. From Fig. 6 it can also be seen that the stripping loss is almost constant across the beam from the SINGAP accelerator, while a significant decrease occurs from centre to corner with the MAMuG accelerator. This occurs because of the greater importance of the lateral conductance relative to the axial conductance in the MAMuG accelerator. The result is a significant density decrease across beam and a high lateral gas flow compared to the axial gas flow. Fig. 8 shows the gas flow distribution for the two accelerator concepts. In the MAMuG case only ~20% of the molecules entering the space between electrode support structures flow out of the accelerator edges at the first attempt, and 80% return back to the beam path region. Nevertheless, because the conductance through the apertures in the sequence of 5 acceleration grids is low, 90% of the total gas escapes laterally from the MAMuG accelerator.





b)

Fig. 8. Gas flow through lateral grid support structure. a) for the MAMuG accelerator, b) for the SINGAP accelerator. The pressure outside of the accelerator is also shown. The gas temperature in the ion source was assumed to be 1000 K.

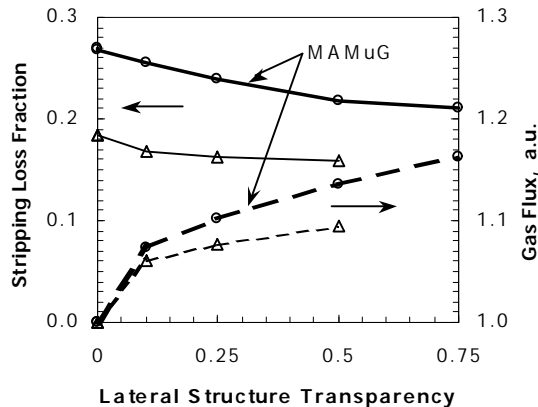


Fig. 9. Stripping loss and relative required gas flux for different transparencies of the support structure.

In both accelerators stripping mainly arises in the first two gaps where the negative ion energy is low and the gas density is high, see Fig. 5. In MAMuG 70% of the gas escapes before the  $-600$  kV electrodes. Paying more attention to the axial transparency of the grid support structure in MAMuG can reduce the gas density, hence the stripping losses, in this region, but at the expense of increasing the gas flow, see Fig. 9. Special attention has to be paid to ensure the highest possible transparency of the grounded grid supporting flange of the MAMuG accelerator as all the gas that escapes laterally from the accelerator (90% of the source gas) must flow through that flange.

Calculations show that, for the MAMuG accelerator, increasing the transparency of the electrodes support structure for better gas pumping should reduce the stripping loss (although it is always larger than with the SINGAP accelerator), at the expense of increasing the source gas flow. If a transparency of 40 to 50% could be achieved, the gain is considerable, see Fig. 9. The consequent increase in gas flow would be 12 to 15%, which should be acceptable. (Note that in the models considered only the support structure surfaces perpendicular to the

beam direction were considered to be partly transparent. Increasing the transparency of other surfaces could lead to an additional decrease in the stripping loss.)

Free electrons and partially accelerated neutrals are generated in the accelerator by stripping collisions. Electrons and positive ions are also created by the ionisation of the background gas by the accelerated negative ions or by their fast atoms created by the aforementioned stripping reactions. Calculations show that the main contribution to the secondary charged particles flux comes from the stripped electrons. The density of the stripped electron generation along the beam path in the accelerator is shown in Fig. 10.

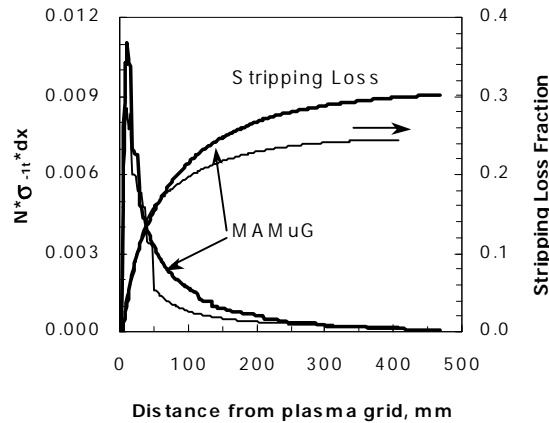


Fig. 10. Electron production rate from collisions of beam particles with gas in the MAMuG and SINGAP accelerators.

#### 4.4 Sensitivity to dissociation of the source gas

It is known, that some fraction of the gas leaving the arc chamber is in the form of D (or H) atoms. That fraction depends on the arc discharge parameters and can be of the order of 20% of the total particle flow from arc chamber. Stripping of negative ions in collisions with these atoms is a resonance charge exchange, hence it is very efficient at low energies. (This has been ignored in the calculations presented above.) At 8 keV/nucleon the cross section is close to that for stripping in collisions with molecules, while for decreasing energy down to 0.1 keV the stripping on atoms increases  $\approx 8$  fold, whereas the stripping on molecules decreases slightly. As the gas density in the accelerator is high where the beam energy is low (see above), this means the contribution of atoms to the stripping loss could be important.

Now the actual atomic fraction is unknown<sup>1</sup>, so the sensitivity of the stripping loss to the atomic fraction has been examined. To assess the loss it is necessary to know the recombination coefficient of the atoms on the surface of the grids and the grid supports,  $A_{rec}$ . Fig. 11 shows the stripping loss on the D atoms for the “virtual” case when the gas flow is 100% flow atomic. (The loss on the D<sub>2</sub> created by recombination is not shown). It can be seen that the stripping on atoms becomes small if the recombination coefficient is  $>0.1$ . This is due to the large number of collisions in the first gap with the grids and grid support

<sup>1</sup> Recent spectroscopic measurements performed by U. Fanz on beam source KAMABOKO-III (MANTIS, CEA Cadrahe), have shown that atomic/molecule ratio in front of extraction apertures is of  $H/H_2 \approx 0.5$  and gas temperature more than 2000 K.

structure, with the resulting recombination of the atoms. It was found that a negligible fraction of the atoms flows into the second gap.

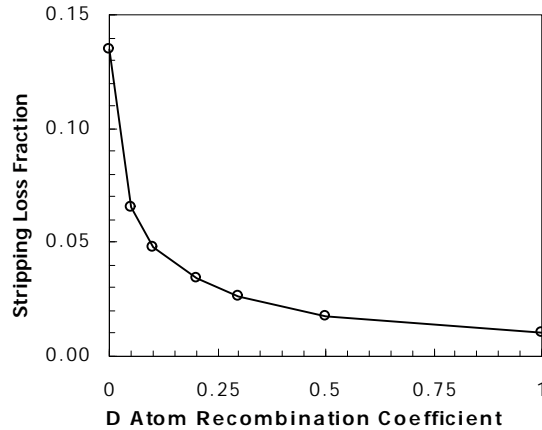


Fig. 11. Stripping loss on 100% atomic gas from the arc chamber. Stripping loss of  $D^+$  ions in collisions only with slow D atoms as function of recombination coefficient of slow D atoms. The temperature of the H atoms entering the accelerator was taken as 1000 K.

## 5 Paschen breakdown in and around the accelerator

It has been shown that "Paschen" breakdown occurs when the applied voltage exceeds some critical value, that value being a function of the product of the pressure and the distance,  $pd$ , between the electrodes between which the breakdown might occur. The data shown in Fig. 8 allow the safety against Paschen breakdowns between the electrodes and between the edge of the accelerator and the grounded vacuum chamber wall. Experiments carried at JAERI have shown that breakdowns occur for voltages  $\geq 200$  kV if the product  $pd > 0.2$  Pa.m ( $p$ : pressure,  $d$ : distance) [12]. The data from Fig. 8 show that  $pd$  will lie in the range 0.007 to 0.02 Pa.m in the MAMuG accelerator (first value for  $d=0.32$  m – gap between electrodes, second for  $\sim 1$  m distance between accelerator edges and the vessel wall), and respectively in the range 0.006 to 0.017 Pa.m in the SINGAP accelerator. These values satisfy the aforementioned requirement.

## Conclusions

A 3D Monte Carlo code has been developed to describe the gas behaviour in the ITER beam sources and applied to both the MAMuG and SINGAP variants of accelerator proposed for the ITER beam source. These calculations give values of gas density distribution, gas flow, stripping loss, and electron generation dependencies for different regions of the beam source.

- The stripping loss and gas flow from the ITER BS for the main possible cases of the reference geometry are summarised in Table 1.

Table 1. **Stripping loss and gas flow in the ITER beam sources**

The background density due to the gas from the neutraliser is assumed to be  $4 \times 10^{18}$  molecules/m<sup>3</sup>. The same accelerator grid geometry is assumed for the two gases.

Operation mode	MAMuG			SINGAP		
	Stripping loss in the centre (%)	Stripping loss in the corner (%)	Source gas flow (Pa m <sup>3</sup> s <sup>-1</sup> )	Stripping loss in the centre (%)	Stripping loss in the corner (%)	Source gas flow (Pa m <sup>3</sup> s <sup>-1</sup> )
H <sup>-</sup> at 1 MeV	24	20	1.28	18	17	1.73
D <sup>-</sup> at 1 MeV	30	25	0.91	22	21	1.23

- The calculated stripping loss for MAMuG is 2 to 3% larger than that calculated by M. Hanada for the vacuum insulated BS [13]. This small difference is possibly due to the lower lateral structure transparency for the grids and grid support structure used for the calculations presented here.
- Sensitivity analyses have been performed to assess the influence on the stripping loss of:
  - the temperature of the gas leaving the arc chamber,
  - the thermal accommodation in collisions with the accelerator structure,
  - the atomic fraction leaving the arc chamber,
  - the transparency of the lateral electrode supporting structure to gas flow.
- The stripping loss in SINGAP is found to be always less than in MAMuG, and the gas flow is slightly higher.
- It may be possible to reduce the stripping loss in MAMuG by improving the lateral pumping by using plates partially transparent to the gas flow for the grid support structure.
- The number of collisions of gas particles with electrodes before they leave the BS is large ( $\gg 1$ ). As a consequence the influence of the temperature of the gas and the atomic fraction leaving the arc chamber is small unless the accommodation or recombination coefficient is  $\ll 1$ .
- The data obtained with this code provide the basis for the calculation of secondary particle power loads in the accelerators, including secondary electrons, and neutrals and positive ions created in the accelerators (double stripping and ionisation).

## Acknowledgements

The authors would like to thank Dr. A. Panasenkov, for encouragement and support, Dr. T. Inoue and Dr. M. Hanada for useful discussions, and Dr. H.P.L de Esch for the potential distributions in the MAMuG and SINGAP accelerators that were used in this paper.

## References

- 
- [1] R.S. Hemsworth *et al.*, "Neutral Beams for ITER". Rev.Sci.Instr, 67 (3) (1996) 1120-1125.
  - [2] R.S. Hemsworth *et al.*, "ITER Neutral Beam Injector Design". 16<sup>th</sup> IAEA Fusion Energy Conference, Montreal, Canada, 7-11 October 1996, IEAA-CN-64/FP-18.

- 
- [3] T. Inoue, E. di Pietro, M. Hanada, R. S. Hemsworth, A. Krylov, V. Kulygin, P. Massmann, P. L. Mondino, Y. Okumura, A. Panasenkov, E. Speth, and K. Watanabe. "Design of neutral beam system for ITER-FEAT", . Fusion Engineering and Design, 56-57 (2001) 517-521.
- [4] R.S. Hemsworth, "Long pulse neutral beam injection", Nuclear Fusion, 43 (2003) 1-11.
- [5] K. Watanabe, *et al.*, "Hydrogen Negative Ion Beam Acceleration in Multi-aperture Five Stager Electrostatic Accelerator", Rev. Sci. Instr., 71 (2) (2000) 1231-1233.
- [6] H.P.L. de Esch, R. Hemsworth and P. Massmann, "SINGAP: The European Concept for Negative Ion Acceleration in the ITER Neutral Injectors", Rev. Sci. Instr. 73 (2) (2002) 1045-1047.
- [7] T. Inoue, K. Miyamoto, M. Mizuno, Y. Okumura and Y. Ohara, "A merging pre-accelerator for high current H<sup>-</sup> ion beams", Rev. Sci. Instr. 65 (7) (1995) 3859-3863.
- [8] K. Kiatani, *et al.*, "Measurement of Velocity Distribution Functions of Neutral Particles in Ion Source Plasma", Rev. Sci. Instr. 73 (2) (2002) 958-960.
- [9] U. Frantz, private communication.
- [10] H.P.L de Esch, private communication.
- [11] Atomic Data for Controlled Fusion Research, ORNL-5207, Internet site: <http://www-cfadc.phy.ornl.gov/redbooks>.
- [12] K. Watanabe *et al.*, "Development of a large volume negative-ion source for ITER neutral beam injector", Rev. Sci. Instr., 73 (2) (2002) 1090-1093.
- [13] M Hanada *et al.*, "Development of negative ion source for the ITER neutral beam injector", Fusion Engineering and Design, 56-57 (2001) 505-509.